

Bayesian Nonparametric Estimation for Point Processes with Spatial Homogeneity: A Spatial Analysis of NBA Shot Locations

Fan Yin

Microsoft

Jieying Jiao

Department of Statistics, University of Connecticut

Guanyu Hu

Department of Statistics, University of Missouri

and

Jun Yan

Department of Statistics, University of Connecticut

November 24, 2020

Abstract

Basketball shot location data provide valuable summary information regarding players to coaches, sports analysts, fans, statisticians, as well as players themselves. Represented by spatial points, such data are naturally analyzed with spatial point process models. We present a novel nonparametric Bayesian method for learning the underlying intensity surface built upon a combination of Dirichlet process and Markov random field. Our method has the advantage of effectively encouraging local spatial homogeneity when estimating a globally heterogeneous intensity surface. Posterior inferences are performed with an efficient Markov chain Monte Carlo (MCMC) algorithm. Simulation studies show that the inferences are accurate and that the method is superior compared to the competing methods. Application to the shot location data of 20 representative NBA players in the 2017-2018 regular season offers interesting insights about the shooting patterns of these players. A comparison against the competing method shows that the proposed method can effectively incorporate spatial contiguity into the estimation of intensity surfaces.

Keywords: Field goal attempts, Dirichlet process mixture, Markov random field, MCMC, Sports analytics

1 Introduction

Quantitative analytics have been a key driving force for advancing modern professional sports, and there is no exception for professional basketball (Kubatko et al., 2007). In professional basketball, analyses of shooting patterns offer important insights about players’ attacking styles and shed light on the evolution of defensive tactics, which has aroused substantial research interests from the statistical community (e.g., Reich et al., 2006; Miller et al., 2014; Jiao et al., 2019; Hu et al., 2020b). As shot location data are naturally represented by spatial points, developments of novel methods for analyzing spatial point patterns are of fundamental importance.

The literature on spatial point pattern data is voluminous (see, e.g., Illian et al., 2008; Diggle, 2013; Guan, 2006; Guan and Shen, 2010; Baddeley, 2017; Jiao et al., 2020). The most frequently adopted class of models in empirical research is nonhomogeneous Poisson processes (NHPP), or more generally, Cox processes, including log-Gaussian Cox process (Møller et al., 1998). Such parametric models impose restrictions on the functional forms of underlying process intensity, which can suffer from underfitting of data when there is a misfit between the complexity of the model and the data available. In contrast, nonparametric approaches provide more flexibility compared to parametric modeling as the underfitting can be mitigated by using models with unbounded complexity.

Several important features of the shot location data need to be captured in any realistic nonparametric method. First, near regions are highly likely to have similar intensities. This makes that certain spatial contiguous constraints on the intensity surface are desirable. Existing method mixture of finite mixtures (MFM) of nonhomogeneous Poisson processes (Geng et al., 2019) is lack of this aspect. Second, spatial contiguous constraints should not dominate the intensity surface globally (Hu et al., 2020a; Zhao et al., 2020). This is because two spatially disconnected regions that are sufficiently similar with respect to the intensity values can still belong to the same cluster. For example, a player may shoot equally frequently at the two corners due to the symmetry of the court, which is not well accommodated by the penalized method (Li and Sang, 2019). Finally, the extent to which the spatial contiguous affects the intensity surface may differ from player to player, and needs to be learned from the data.

To address these challenges, we consider a spatially constrained Bayesian nonparametric method for point processes to capture the spatial homogeneity of intensity surfaces. Our contributions

are three-fold. First, we develop a novel nonparametric Bayesian method for intensity estimation of spatial point processes. Compared to existing methods, the proposed approach is capable of capturing both locally spatially contiguous clusters and globally discontinuous clusters and the number of clusters. Second, an efficient Markov chain Monte Carlo (MCMC) algorithm is designed for our model without complicated reversible jump MCMC. Lastly, we gain important insights about the shooting behaviors of NBA players based on an application to their shot location data.

The rest of the paper is organized as follows. In Section 2, we introduce and visualize the shot charts of several representative NBA players from the 2017–2018 regular season. In Section 3, we introduce spatial point processes for field goal attempts and develop a nonparametric Bayesian method for capturing the spatial homogeneity of intensity surface. Detailed Bayesian inference procedures, including a collapsed Gibbs sampler and a post MCMC inference method, are presented in Section 4. Extensive simulation studies are reported in Section 5. The method is applied to 20 key NBA players’ shot location data from the 2017-2018 regular season in Section 6. Section 7 concludes with a discussion. For ease of exposition, additional results are relegated to the Supplementary Material.

2 NBA Shot Location Data

Shot chart data for NBA players from the 2017–2018 regular season were retrieved from the official website of NBA `stats.nba.com`. The data for each player contain information about all his shots in regular season including game date, opponent team name, game period when each shot was made (4 quarters and a fifth period representing extra time), minutes and seconds left, success indicator (0 represents missed and 1 represents made), action type (like “Cutting dunk shot”, “Jump shot”, etc.), shot type (2-point or 3-point shot), shot distance, and shot location coordinates. From the data, the half court is positioned on a Cartesian coordinate system centered at the center of rim, with x ranging from -250 to 250 and y ranging from -50 to 420 , both with unit of 0.1 foot (ft), as the size of an actual NBA basketball half court is $50 \text{ ft} \times 47 \text{ ft}$.

We visualize and summarize the shot data of four key players, Stephen Curry, James Harden, Kevin Durant and DeMar DeRozan. Figure 1 shows their field goal attempts’ locations and Table 1 summarizes their other field goal attempts information. As we can see from the plots, most of the shots are made either close to the rim or right outside the arc (i.e., 3-point line). This is in line

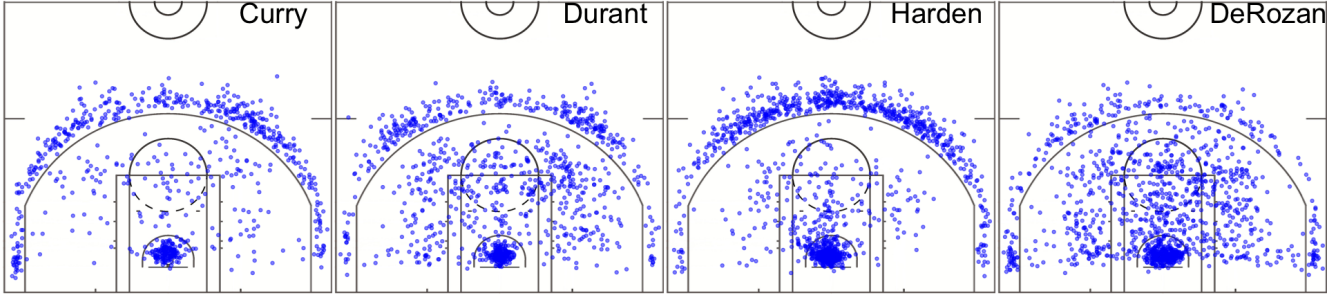


Figure 1: Shot data Display. On half court image, each point represents one shot. From left to right: Stephen Curry, Kevin Durant, James Harden, DeMar DeRozan.

Table 1: Shot data summary. Period is for the 1st, 2nd, 3rd, 4th quarter and the extra time.

Player	Shot Count	2PT shot percentage (%)	Period percentage (%)
Stephen Curry	753	42.6	(35.0, 20.6, 34.3, 9.7, 0.4)
James Harden	1306	50.2	(28.7, 22.4, 27.9, 20.8, 0.3)
Kevin Durant	1040	66.5	(30.8, 23.8, 30.6, 14.6, 0.3)
DeMar DeRozan	1274	79.9	(29.1, 28.6, 33.3, 17.3, 1.6)

with the recent trend in the basketball development since it is more efficient for players to pursue higher success rates near the rim or go after higher rewards by making 3-point shots.

3 Model

3.1 NHPP

Spatial point process models provide a natural framework for capturing the random behavior of event location data. Let $\mathbf{S} = \{\mathbf{s}_1, \mathbf{s}_2, \dots, \mathbf{s}_N\}$ with $\mathbf{s}_i = (x_i, y_i)$, $i = 1, \dots, N$, be the set of observed locations in a pre-defined, bounded region $\mathcal{B} \subseteq \mathcal{R}^2$. Let the underlying stochastic mechanism that gives rise to the observed point pattern \mathbf{S} be denoted as spatial point process \mathbf{Y} . Process $N_{\mathbf{Y}}(A) = \sum_{i=1}^N \mathbb{1}(\mathbf{s}_i \in A)$ is a counting process associated with \mathbf{Y} , which counts the number of points falling into area $A \subseteq \mathcal{B}$.

The NHPP model assumes conditionally independent event locations given the process intensity

$\lambda(\mathbf{s})$. For an NHPP, the number of events in area A , $N_{\mathbf{Y}}(A)$, follows Poisson distribution with rate parameter $\lambda(A) = \int_A \lambda(\mathbf{s})d\mathbf{s}$. In addition, $N_{\mathbf{Y}}(A_1)$ and $N_{\mathbf{Y}}(A_2)$ are independent if two areas $A_1 \subseteq \mathcal{B}$ and $A_2 \subseteq \mathcal{B}$ are disjoint. Given the observed point pattern \mathbf{S} on fixed region \mathcal{B} , the likelihood of the NHPP model is

$$\frac{\prod_{i=1}^N \lambda(\mathbf{s}_i)}{\exp(\int_{\mathcal{B}} \lambda(\mathbf{s})d\mathbf{s})}, \quad (3.1)$$

where $\lambda(\mathbf{s}_i)$ is the intensity function evaluated at location \mathbf{s}_i . The NHPP reduces to a homogeneous Poisson process (HPP) when $\lambda(\mathbf{s})$ is constant over the entire study region \mathcal{B} , and it is synonymous with *complete spatial randomness* (CSR).

3.2 Nonparametric Bayesian Methods for NHPP

As the CSR assumption over the entire study region rarely holds in real-world problems, and to simplify the potentially overcomplicated problem induced by complete non-homogeneity on intensity values, Teng et al. (2017) proposed to approximate the intensity function $\lambda(\mathbf{s})$ by a piecewise constant function. Specifically, the study region \mathcal{B} is partitioned into n disjoint sub-regions and the intensity over each sub-region is assumed to be constant. Let A_1, A_2, \dots, A_n be a partition of \mathcal{B} , i.e., $\cup_{i=1}^n A_i = \mathcal{B}$ and $A_i \cap A_j = \emptyset, \forall i \neq j$. For each region $A_i, i = 1, \dots, n$, we have $\lambda(\mathbf{s}) = \lambda_i, \forall \mathbf{s} \in A_i$. Therefore, the likelihood (3.1) can be written as

$$\prod_{i=1}^n f_{\text{poisson}}(N_{\mathbf{Y}}(A_i) | \lambda_i \mu(A_i)), \quad (3.2)$$

where $\mu(A_i = \int_{A_i} 1d\mathbf{s})$ is the area of sub-region A_i $f_{\text{poisson}}(\cdot | \lambda)$ is the probability mass function of the Poisson distribution with rate parameter λ . For ease of notation, we use $N(A_i)$ for $N_{\mathbf{Y}}(A_i)$ in the sequel.

The heterogeneity in the intensity function across different sub-regions can be naturally represented through a latent clustering structure. The conventional finite mixture modeling framework (McLachlan and Basford, 1988; Bouveyron et al., 2019) assumes that the heterogeneity can be characterized by a discrete set of subpopulations or clusters, such that the points located in the sub-regions belonging to any given subpopulation tend to be produced by similar intensities. The selection of the number of clusters (or components) in finite mixture models are often recasted as statistical model selection problems which can be solved using information criteria (Fraley and Raftery, 2002) or cross-validation (Fu and Perry, 2020), among others. Despite many successful

applications in empirical research, such model selection procedures are fraught with in that they ignore the uncertainty in the number of clusters, which may in turn lead to increased erroneous cluster assignments.

The Chinese restaurant process (CRP) (Pitman, 1995; Neal, 2000) mixture models is a class of Bayesian nonparametric approaches that offer a powerful alternative to conventional finite mixture models. Under CRP mixture models, the latent cluster indicator variables $\mathbf{Z} = (Z_1, Z_2, \dots, Z_n)$ are distributed according to a CRP, which is defined through the following conditional distributions or a Pólya urn scheme (Blackwell and MacQueen, 1973)

$$\Pr(Z_i = c | Z_j, j < i; \alpha) \propto \begin{cases} |c|, & c \text{ is an existing cluster label } c, \\ \alpha, & \text{otherwise,} \end{cases} \quad (3.3)$$

where $|c|$ refers to the size of cluster labeled c , and α is the concentration parameter of the underlying Dirichlet process (DP). Specifically, Equation (3.3) implies that the trivial partition $\{\{1\}\}$ is obtained with probability 1 at the beginning, and one new element is either added to one of the existing blocks of the partition \mathcal{C}_n with probability $|c|/(n + \alpha)$ or to the partition \mathcal{C}_n as a new singleton block with probability $\alpha/(n + \alpha)$ in subsequent steps. More intuitively, we may think of customers choosing tables in a restaurant, where the first customer always chooses the first table and the i th customer chooses the first unoccupied table with probability $\alpha/(n + \alpha)$ and an occupied table with probability proportional to the number of customers currently sitting at that table (i.e., how popular this table is), $|c|/(n + \alpha)$.

The CRP mixture models admit the uncertainty in the number of clusters and circumvents the model selection problems by allowing the number of clusters and cluster assignments to be inferred simultaneously. To facilitate statistical inference, it is often helpful to consider the full conditional distributions of Z_i , $i = 1, \dots, n$ under the CRP,

$$\Pr(Z_i = c | \mathbf{Z}_{-i}, \alpha) \propto \begin{cases} n_c(\mathbf{Z}_{-i}), & \text{at an existing cluster label } c, \\ \alpha, & \text{at a new cluster,} \end{cases} \quad (3.4)$$

where $\mathbf{Z}_{-i} = \{Z_j : j \neq i\}$, and $n_c(\mathbf{Z}_{-i}) = \sum_{i=1, i \neq j}^n \mathbb{1}(Z_i = c)$ is the number of observations in cluster labeled c without the i th observation. That is, each Z_i is either a new label with probability proportional to α , or an existing label c with probability proportional to the observations assigned

to cluster c , $n_c(\mathbf{Z}_{-i})$. The concentration parameter α controls the distribution of the number of clusters, with smaller values of α favoring smaller number of clusters *a priori*.

We formulate a Bayesian hierarchical CRP-NHPP model as

$$\begin{aligned} Z_1, \dots, Z_n &\sim \text{CRP}(\alpha), \\ \lambda_1, \dots, \lambda_K &\stackrel{i.i.d.}{\sim} \text{Gamma}(a, b) \\ N(A_i) \mid \boldsymbol{\lambda}, Z_1, \dots, Z_n &\sim \text{Poisson}(\lambda_{Z_i} \mu(A_i)), \text{ independently for } i = 1, \dots, n, \end{aligned} \tag{3.5}$$

where K is the number of components of the piecewise constant function, $\boldsymbol{\lambda} = (\lambda_1, \lambda_2, \dots, \lambda_K)$ is the vector of the unique values of the intensity function, $\text{Gamma}(a, b)$ is the gamma distribution with shape a and rate b , (a, b, α) are hyperparameters for the prior distributions, and *i.i.d.* stands for independent and identically distributed. The hyperparameters can be specified according to the *a priori* information available for the practitioners.

An alternative model which will be used as a benchmark for comparison is the MFM of NHPP (MFM-NHPP) (Geng et al., 2019). This model is built upon the MFM modeling framework (Miller and Harrison, 2018) to mitigate the potential *inconsistency* in estimating the number of clusters caused by CRP mixture. The MFM-NHPP model is

$$\begin{aligned} K &\sim p_K, \\ \lambda_k &\stackrel{i.i.d.}{\sim} \text{Gamma}(a, b), \quad k = 1, 2, \dots, K, \\ (\pi_1, \dots, \pi_k) \mid K = k &\sim \text{Dirichlet}_k(\alpha, \dots, \alpha), \\ Z_1, \dots, Z_n \mid \pi_1, \dots, \pi_k &\stackrel{i.i.d.}{\sim} \text{Categorical}_k(\pi_1, \dots, \pi_k), \\ N(A_i) \mid \boldsymbol{\lambda}, Z_1, \dots, Z_n &\sim \text{Poisson}(\lambda_{Z_i} \mu(A_i)), \text{ independently for } i = 1, \dots, n, \end{aligned} \tag{3.6}$$

where p_K is the prior distribution on the number of clusters, that is, a probability mass function on $\mathbb{N} = \{1, 2, \dots\}$. Geng et al. (2019) adopt Poisson with mean 1 truncated to be positive for p_K as recommended by Miller and Harrison (2018), which we follow here.

3.3 Incorporating Spatial Homogeneity

Spatial events typically obey the so-called first law of geography, “everything is related to everything else, but near things are more related than distant things” (Tobler, 1970). This means spatial smoothness, also known as spatial homogeneity. To incorporate such spatial homogeneity,

we propose to modify (3.4) by adding a multiplier that encourages the customer to choose the table where many spatial neighbors are also sitting at. In particular, we consider the following full conditionals

$$\Pr(Z_i = c | \mathbf{Z}_{-i}, \alpha, \eta, D) \tag{3.7}$$

$$\propto \begin{cases} n_c(\mathbf{Z}_{-i}) \exp\left(\eta \sum_{j \in \partial(i)} d_{ij} \mathbb{1}(Z_j = c)\right), & c \text{ is an existing cluster labeled } c, \\ \alpha, & \text{otherwise,} \end{cases} \tag{3.8}$$

where D comprises the information on spatial distance and neighbor relationships, $\partial(i)$ represents the set of spatial neighbors of the i th customer (observation), d_{ij} denotes the spatial distance between the i th and the j th customer (observation), and $\eta \geq 0$ is a smoothing parameter controlling the relative weight of spatial homogeneity.

The full conditionals (3.7) can be specified by DP mixtures (DPM) constrained by a Markov random field (MRF) (Orbanz and Buhmann, 2008). Combining the NHPP with the MRF constrained DPM, we have a MRF-DPM-NHPP model

$$\begin{aligned} G &\sim \text{DP}(\alpha, G_0) \\ (\lambda_1, \dots, \lambda_n) &\sim M_{\eta, D}(\lambda_1, \dots, \lambda_n) \prod_{i=1}^n G(\lambda_i) \end{aligned} \tag{3.9}$$

$$N(A_i) \mid \lambda_1, \dots, \lambda_n \sim \text{Poisson}(\lambda_i) \text{ independently for } i = 1, \dots, n,$$

where $DP(\alpha, G_0)$ is a DP with base measure $G_0 \equiv \text{Gamma}(a, b)$ and concentration parameter α , $G(\lambda_i)$ is defined by a single draw from a DP (Ferguson, 1973), and $M_{\eta, D}(\lambda_1, \dots, \lambda_n)$ is a MRF with full conditionals

$$M_{\eta, D}(\lambda_i | \boldsymbol{\lambda}_{-i}) = M_{\eta, D}(\lambda_i | \boldsymbol{\lambda}_{\partial(i)}) \propto \exp\left(\eta \sum_{j \in \partial(i)} d_{ij} \mathbb{1}(\lambda_i = \lambda_j)\right)$$

It is worth noting that the existence of joint distribution $M_{\eta, D}(\lambda_1, \dots, \lambda_n)$ is guaranteed by the Hammersley—Clifford theorem (Hammersley and Clifford, 1971).

The definition of neighborhood $\partial(i)$ is subject to the nature of the data and the modeler’s choice. Common choices include the *rook* contiguity (i.e., the regions which share a border of some length with region i), and the *queen* contiguity (i.e., the regions which share a border of some length or even a point-length border with region i). The smoothing parameter η controls the

extent of spatial homogeneity, with larger values dictating larger extent of spatial homogeneity. The MRF-DPM-NHPP model (3.9) reduces to the CRP-NHPP model (3.5) when $\eta = 0$.

4 Bayesian Inference

In this section, we present an efficient MCMC sampling algorithm for our proposed method, post MCMC inference, and model selection criteria.

4.1 A Collapsed Gibbs Sampler

We introduce latent indicator variables $\mathbf{Z} = (Z_1, \dots, Z_n)$ and denote the parameters in (3.9) as $\Theta = \{\boldsymbol{\lambda}, \mathbf{Z}\}$. The posterior density of Θ is

$$\pi(\Theta|\mathbf{S}) \propto L(\Theta|\mathbf{S})\pi(\Theta)$$

, where $\pi(\Theta)$ is the prior density of Θ , and the likelihood $L(\Theta|\mathbf{S})$ takes the form of (3.1).

We first derive the full conditional distribution for each parameter as follows. The full conditional probability that sub-region A_i belongs to an existing component c , i.e., $\exists j \neq i, Z_j = c$, is

$$\Pr(Z_i = c \mid \mathbf{S}, \mathbf{Z}_{-i}, \boldsymbol{\lambda}) \propto \frac{n_c(\mathbf{Z}_{-i}) \exp\left(\eta \sum_{j \in \partial(i)} d_{ij} \mathbb{1}(Z_j = c)\right) (\lambda_c \mu(A_i))^{N(A_i)}}{n - 1 + \alpha} \frac{(\lambda_c \mu(A_i))^{N(A_i)}}{\exp(\lambda_c \mu(A_i))}. \quad (4.1)$$

The full conditional probability that A_i belongs to a new component, i.e., $\forall j \neq i, Z_j \neq c$, is

$$\begin{aligned} & \Pr(Z_i = c \mid \mathbf{S}, \mathbf{Z}_{-i}, \boldsymbol{\lambda}) \\ & \propto \frac{\alpha}{n - 1 + \alpha} \int \frac{(\lambda_c \mu(A_i))^{N(A_i)}}{\exp(\lambda_c \mu(A_i))} \frac{b^a}{\Gamma(a)} \lambda_c^{a-1} e^{-b\lambda_c} d\lambda_c \\ & = \frac{\alpha}{n - 1 + \alpha} \frac{b^a}{\Gamma(a)} \mu(A_i)^{N(A_i)} \int \lambda_c^{N(A_i)+a-1} e^{-(b+\mu(A_i))\lambda_c} d\lambda_c \\ & = \frac{\alpha b^a \Gamma(N(A_i) + a) \mu(A_i)^{N(A_i)}}{(n - 1 + \alpha)(b + \mu(A_i))^{N(A_i)+a} \Gamma(a)}. \end{aligned} \quad (4.2)$$

Combining (4.1) and (4.2) gives the full conditional distribution of Z_i in the following Proposition.

Proposition 1. Under the model and prior specification (3.9), the full conditional distribution of Z_i , $i = 1, \dots, n$, is

$$\Pr(Z_i = c \mid \mathbf{S}, \mathbf{Z}_{-i}, \boldsymbol{\lambda}, \boldsymbol{\beta}) \propto \begin{cases} \frac{n_c(\mathbf{Z}_{-i}) \exp\left(\eta \sum_{j \in \partial(i)} d_{ij} \mathbb{1}(Z_j = c)\right) (\lambda_c \mu(A_i))^{N(A_i)}}{\exp(\lambda_c \mu(A_i))} & \exists j \neq i, Z_j = c \text{ (existing label),} \\ \frac{\alpha b^a \Gamma(N(A_i) + a) \mu(A_i)^{N(A_i)}}{(b + \mu(A_i))^{N(A_i) + a} \Gamma(a)} & \forall j \neq i, Z_j \neq c \text{ (new label),} \end{cases} \quad (4.3)$$

where \mathbf{Z}_{-i} is \mathbf{Z} with z_i removed, and $\mu(A_i)$ is the area of region A_i .

For the full conditional distribution of λ_k , only data points in the k th component should be considered for simplicity. The full conditional density of λ_k , $k = 1, \dots, K$, is

$$\begin{aligned} q(\lambda_k \mid \mathbf{S}, \mathbf{Z}, \boldsymbol{\lambda}_{-k}) &\propto \frac{\prod_{\ell: \mathbf{s}_\ell \in A_j, Z_j = k} \lambda(\mathbf{s}_\ell)}{\exp\left(\int_{\bigcup_{j: Z_j = k} A_j} \lambda(\mathbf{s}) d\mathbf{s}\right)} \lambda_k^{a-1} \exp(-b\lambda_k) \\ &= \frac{\prod_{\ell: \mathbf{s}_\ell \in A_j, Z_j = k} \lambda_k}{\exp\left(\int_{\bigcup_{j: Z_j = k} A_j} \lambda_k d\mathbf{s}\right)} \lambda_k^{a-1} \exp(-b\lambda_k) \\ &\propto \lambda_k^{N_k + a - 1} \exp\left(-\left(b + \sum_{j: Z_j = k} \mu(A_j)\right) \lambda_k\right), \end{aligned} \quad (4.4)$$

which is the kernel of $\text{Gamma}(N_k + a, b + \sum_{j: Z_j = k} \mu(A_j))$, where $N_k = \sum_{\ell: \mathbf{s}_\ell \in A_j, Z_j = k} 1$ is the number of data points in the sub-regions belonging to the k th component.

Algorithm 1 summarizes the steps of a Gibbs sampling algorithm using the full conditional distributions from (4.3)–(4.4).

Convergence check for the auxiliary variables (Z_1, \dots, Z_n) can be done with the help of the Rand Index (RI) (Rand, 1971). The auxiliary variables themselves are nominal labels which cannot be compared from iteration to iteration. The RI is the proportion of concordant pairs between two clustering results with value of 1 indicating the two results are exactly the same. The trajectory of the RI for successive MCMC iterations provides a visual check for convergence. Further, RI values closer to 1 indicate good agreement in the clustering in the MCMC samples.

4.2 Post MCMC Inference

We carry out posterior inference on the group memberships using Dahl's method (Dahl, 2006), which proceeds as follows.

Algorithm 1 Collapsed Gibbs sampler for MRF-DPM-NHPP.

Input:

Data: point locations \mathbf{s}_i , $i = 1, \dots, N$; sub-regions and their neighbors $\{A_i, \partial(i) : i = 1, \dots, n\}$.

Prior hyperparameters : a, b, α .

Tuning parameter: η .

Burn-in MCMC sample size: B , post-burn-in MCMC sample size: L .

Initial values: $K, Z_1, \dots, Z_n, \boldsymbol{\lambda} = (\lambda_1, \dots, \lambda_K)$, iter = 1.

1: **while** iter $\leq B + L$ **do**

2: Update $\lambda_k | \cdot$, $k = 1, \dots, K$ as

$$\lambda_k | \cdot \sim \text{Gamma} \left(N_k + a, b + \sum_{j:Z_j=k} \mu(A_j) \right)$$

where $N_k = \sum_{\ell: \mathbf{s}_\ell \in A_j, Z_j=k} 1$ is the number of points belonging to the k th component.

3: Update $Z_i | \cdot$, $i = 1, \dots, n$ following Proposition 1.

4: iter = iter + 1.

5: **end while**

Output: Posterior samples $Z_1^{(l)}, \dots, Z_n^{(l)}, \boldsymbol{\lambda}^{(l)}$, $l = B + 1, \dots, B + L$.

1. Define membership matrices $\mathcal{H}^{(l)} = (\mathcal{H}^{(l)}(i, j))_{i, j \in \{1, \dots, n\}} = (\mathbb{1}(Z_i^{(l)} = Z_j^{(l)}))_{n \times n}$, where $l = 1, \dots, L$ indexes the number of retained MCMC draws after burn-in, and $\mathbb{1}(\cdot)$ is the indicator function.
2. Calculate the average membership matrix $\overline{\mathcal{H}} = \frac{1}{L} \sum_{l=1}^L \mathcal{H}^{(l)}$ where the summation is element-wise.
3. Identify the most *representative* posterior sample as the one that is closest to $\overline{\mathcal{H}}$ with respect to the element-wise Euclidean distance $\sum_{i=1}^n \sum_{j=1}^n (\mathcal{H}^{(l)}(i, j) - \overline{\mathcal{H}}(i, j))^2$ among the retained $l = 1, \dots, L$ posterior samples.

Therefore, the posterior estimates of cluster memberships Z_1, \dots, Z_n and model parameters Θ can be based on the draws identified by Dahl's method.

4.3 Selection of Smoothing Parameter

We recast the choice of smoothing parameter $\eta \geq 0$ as a model selection problem. In particular, we consider the deviance information criterion (DIC; Spiegelhalter et al. (2002)), logarithm of the Pseudo-marginal likelihood LPML; Gelfand and Dey (1994)) and Bayesian information criterion (BIC; Schwarz (1978)) as candidates.

The DIC for spatial point process can be derived from the standard DIC in a straightforward manner as

$$\text{Dev}(\Theta) = -2 \left(\sum_{i=1}^N \log \lambda(\mathbf{s}_i) - \int_{\mathcal{B}} \lambda(\mathbf{s}) d\mathbf{s} \right),$$

$$\text{DIC} = 2\overline{\text{Dev}}(\Theta) - \text{Dev}(\hat{\Theta}),$$

where $\overline{\text{Dev}}(\Theta)$ is the average deviance evaluated using each posterior sample of Θ , and $\text{Dev}(\hat{\Theta})$ is the deviance calculated using the point estimation of parameter using Dahl's method.

The LPML for spatial point process can be approximated using the MCMC samples (Hu et al.,

2019)

$$\begin{aligned}\widehat{\text{LPML}} &= \sum_{i=1}^N \log \tilde{\lambda}(\mathbf{s}_i) - \int_{\mathcal{B}} \bar{\lambda}(\mathbf{s}) d\mathbf{s}, \\ \tilde{\lambda}(\mathbf{s})_i &= \left(\frac{1}{M} \sum_{t=1}^M \lambda(\mathbf{s}_i | \Theta_t)^{-1} \right)^{-1}, \\ \bar{\lambda}(\mathbf{s}) &= \frac{1}{M} \sum_{t=1}^M \lambda(\mathbf{s} | \Theta_t),\end{aligned}$$

where Θ_t denotes the t -th posterior sample of parameters with a total length of M .

The BIC is derived naturally from its general definition

$$\begin{aligned}\text{BIC}(\Theta) &= -2 \log L(\Theta) + \hat{K} \log N, \\ \log L(\Theta) &= \sum_{i=1}^N \log \lambda(\mathbf{s}_i) - \int_{\mathcal{B}} \lambda(\mathbf{s}) d\mathbf{s},\end{aligned}$$

where \hat{K} denotes the estimated number of components of the piecewise constant intensity function.

5 Simulation Studies

In this section, we report simulation studies to examine the performance of the MRF-DPM-NHPP model and the proposed Gibbs sampling algorithm. In each setting, we compare the results to that of MFM-NHPP To to show that the MRF-DPM-NHPP model indeed leads to improvements.

5.1 Design

Consider a study region $\mathcal{B} = [0, 20] \times [0, 20]$ partitioned into $n = 400$ squares of unit area, $\{A_i\}_{i=1}^n$. The data generating model was set to be NHPP($\lambda(\mathbf{s})$) with a piecewise constant intensity $\lambda(\mathbf{s})$ over \mathcal{B} . Three settings were considered for $\lambda(\mathbf{s})$; see Table 2. The “ground-truth” intensity surfaces of the three settings are displayed in the leftmost column of Figure 2. The first two settings with the different numbers of clusters are similar with the simulation setups in Geng et al. (2019). The third setting contains both spatially contiguous and discontinuous clusters. The point patterns were generated using the `rpoispp()` function from package `spatstat` (Baddeley and Turner, 2005). For each setting, we generated 100 replicates.

Table 2: Simulation settings for the piecewise constant intensity function.

	λ	Number of components in λ	Number of grid boxes
Setting 1	(0.2, 4, 12)	3	(90, 211, 99)
Setting 2	(0.2, 1, 4, 8, 16)	5	(80, 80, 80, 80, 80)
Setting 3	(0.2, 4, 10, 20)	4	(90, 145, 66, 99)

The prior distributions were specified as in (3.9), with hyperparameters $a = b = \alpha = 1$. The smoothing parameter $\eta \geq 0$ took values on an equally-spaced grid $\eta = \{0, 0.5, \dots, 7.5, 8\}$, of which the optimal value is chosen via the model selection criteria introduced in Section 4.3. The neighboring structure was defined based on rook contiguity, and we treat all neighbors equally by letting $d_{ij} = 1, \forall j \in \partial i$. Each MCMC chain was run for a total of 4000 iterations with random starting values, where the first 2000 draws were discarded as burn-in. The remaining 2000 draws were thinned by 10 and stored for posterior inference. We used Dahl’s method (Dahl, 2006) to identify the most representative draw from the retained posterior draws as the posterior point estimate.

5.2 Results

We evaluate the results of simulation studies on the following aspects, (i) probability of choosing the correct number of clusters, (ii) clustering accuracy quantified by the RI, and (iii) estimation accuracy of the intensity surface.

Table 3 (left block) shows the proportion of times the true number of components is identified under different model selection criteria for each simulation setting. Obviously, $\eta = 0$ never recovered the true number of clusters, suggesting that taking spatial contiguity information into account is crucial. For MRF-DPM-NHPP, BIC appears to be better than DIC and LPML as the BIC-selected *optimal* η recovered the true number of clusters considerably more frequently ($> 70\%$). Although MFM-NHPP seems to be very competitive in terms of identifying the true number of components under setting 1, MRF-DPM-NHPP with smoothing parameter η selected by BIC offers substantially better performance under setting 2 and setting 3. A further investigation revealed that setting $\eta = 0$ always produced overly large numbers of redundant clusters,

Table 3: Proportion of times the true number of cluster is identified, and average RI across 100 replicates for each simulation setting, under MFM-NHPP, and MRF-DPM-NHPP with $\eta = 0$, optimal η selected by BIC, DIC and LPML.

	Accuracy of \hat{K}					Average RI					
	MRF-DPM-NHPP					MFM-NHPP	MRF-DPM-NHPP				MFM-NHPP
	$\eta = 0$	BIC	DIC	LPML			$\eta = 0$	BIC	DIC	LPML	
Setting 1	0.00	0.75	0.21	0.22	0.95	0.619	0.974	0.890	0.891	0.905	
Setting 2	0.00	0.82	0.61	0.63	0.20	0.803	0.991	0.982	0.982	0.775	
Setting 3	0.00	0.71	0.10	0.11	0.56	0.739	0.992	0.939	0.942	0.870	

while DIC and LPML failed more gracefully with wrong numbers of clusters that often fall into the approximate range (A histogram of \hat{K} is available in the Supplementary Material).

To assess the clustering performance, we examine the average RI over the 100 replicates. Because the “ground-truth” class labels are known in the simulation studies, the RIs were calculated by comparing the MCMC iterations with the truth as a measure of clustering accuracy. As shown in Table 3 (right block), MRF-DPM-NHPP with smoothing parameter η selected by BIC yields the highest clustering accuracy. Although Despite being more capable of identifying the true number of clusters, the clustering accuracy of MFM-NHPP is worse than that of MRF-DPM-NHPP with BIC under setting 1, which suggests that MFM-NHPP might happen to get the number of clusters right by allocating the regions into wrong clusters. For the remainder of this paper, we focus on the results that correspond to optimal η selected by BIC.

We next summarize accuracy in estimating the intensity surfaces. Figure 2 displays the averages of the median, 2.5th percentile, and 97.5th percentile of the estimated intensity surface obtained with the optimal η selected by BIC from the 100 replicates, in comparison with the true surfaces, for the three settings. The median surface agrees with true surface well in all three settings. The average surfaces of the 2.5th and 97.5th percentiles of the 100 replicates have higher uncertainties occasionally at the boundaries where the true intensities jump, but in general are not far from the true surfaces. Figure 3 shows the absolute value of relative bias of element-wise posterior mean estimates under the MFM-DPM-NHPP model and the MFM-NHPP model. The proposed

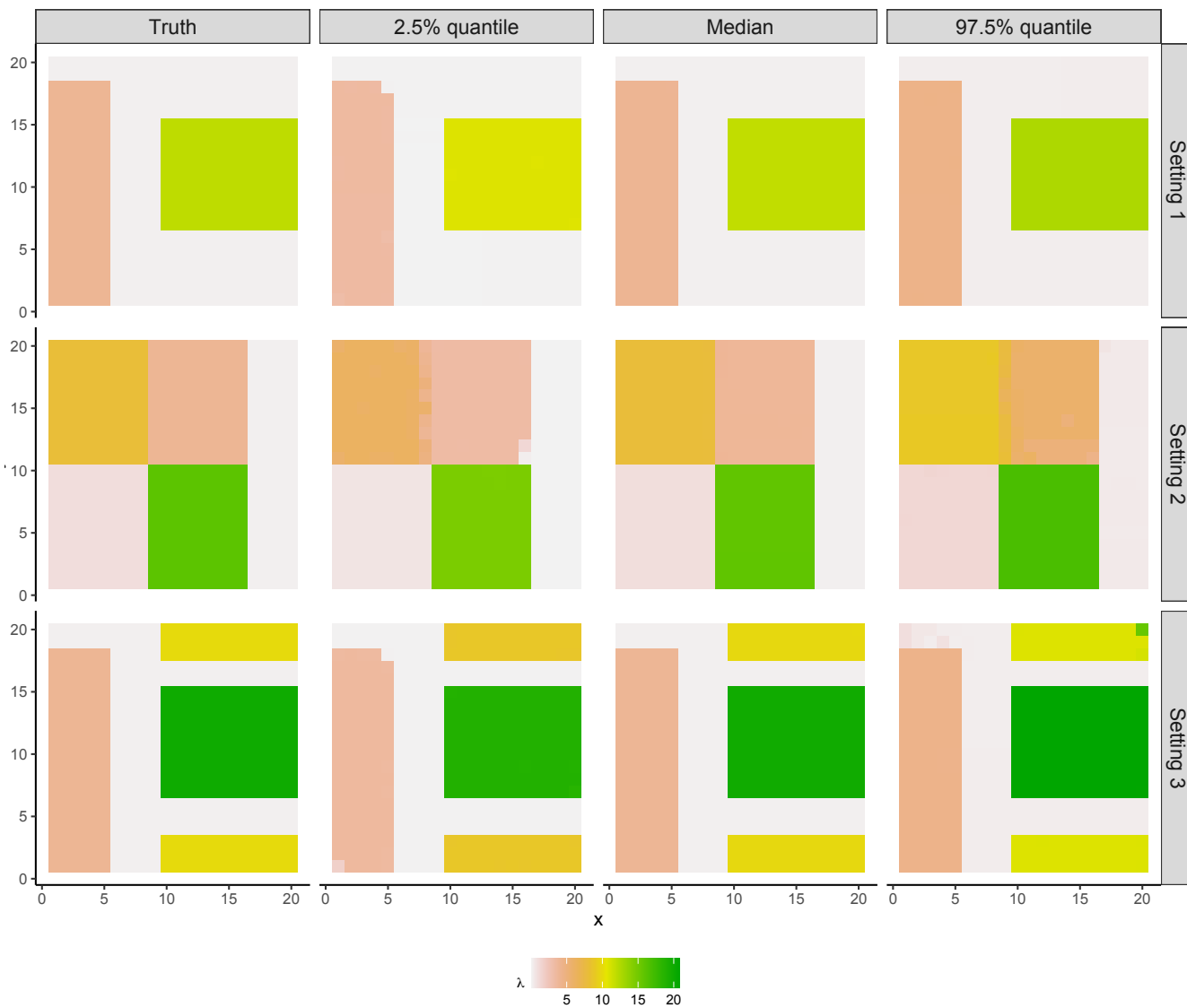


Figure 2: Simulation configurations for intensity surfaces, with fitted intensity surfaces. Element-wise median and quantiles are calculated out of 100 replicates.

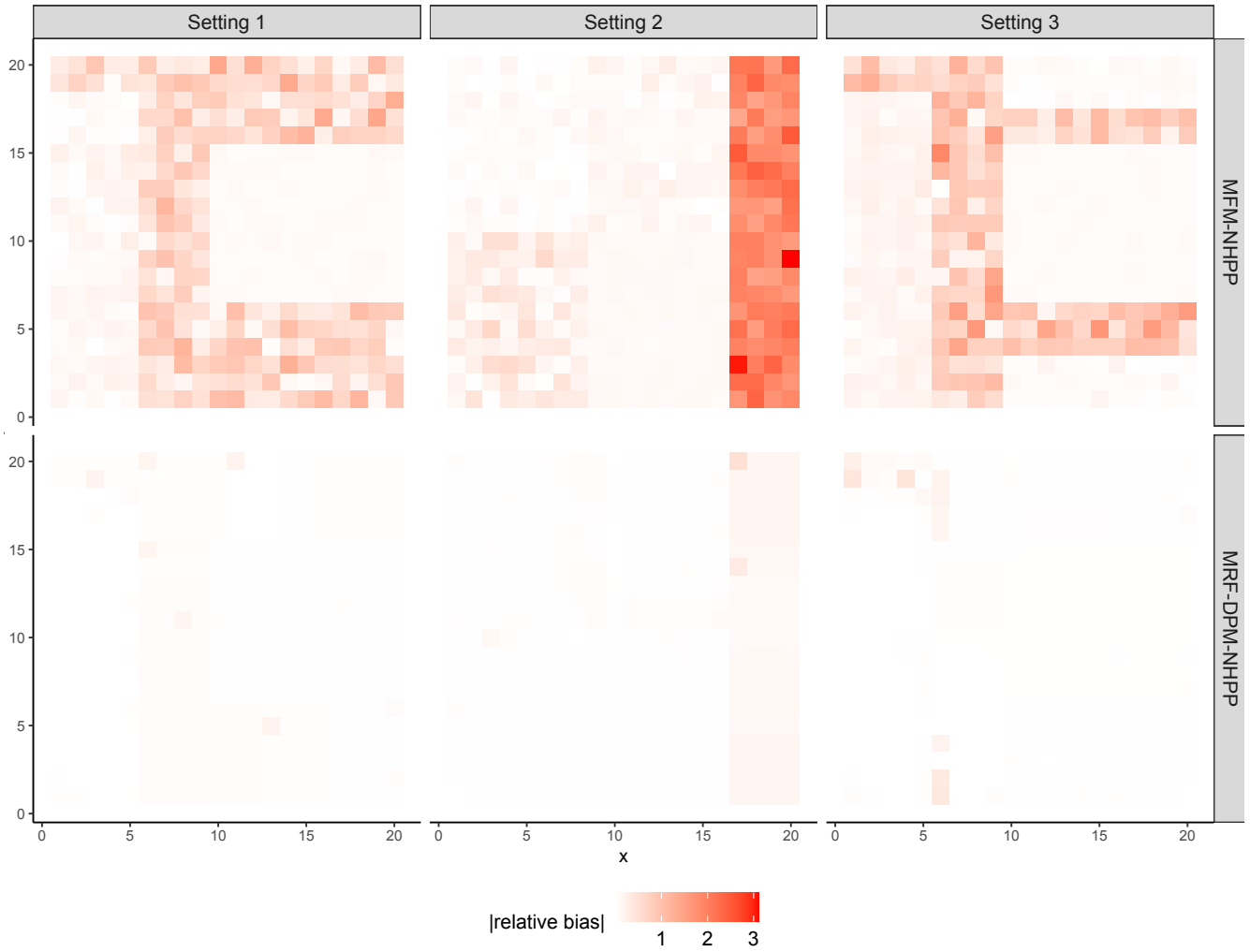


Figure 3: Absolute value of relative bias of element-wise posterior mean estimates for intensity surfaces.

method leads to substantially smaller bias than the competing method, especially for sub-regions with low true underlying intensity values and/or sub-regions at the boundaries. The advantage of the proposed method comes from leveraging the spatial contiguity in the presence of spatial homogeneity.

The overlaid traceplots of RI (available in Supplementary Material) indicate that the chains converge very fast, and stabilize after 2000 iterations, regardless of the settings. This observation justifies our choice of the MCMC setting.

In summary, the simulation studies confirm the advantages of the MRF-DPM-NHPP model and the validity of the proposed Gibbs sampling algorithm. The results also suggest that BIC is better than DIC and LPML in selecting the smoothing parameter η in the studied settings. Compared to the benchmark MFM-NHPP model, the MRF-DPM-NHPP model is superior in clustering accuracy and has an advantage on identifying the true number of components under more complex settings.

6 Professional Basketball Data Analysis

We applied the MRF-DPM-NHPP model to study the shot data for NBA players in the 2017-2018 NBA regular season described in Section 2. In particular, we focus on 20 all-star level players that are representative of their positions (Table 4). The study region is a rectangle covering the first 75% of the half court ($50 \text{ ft} \times 35 \text{ ft}$) as the shots made outside this region are often not part of the regular tactics. This rectangle was divided into $50 \times 35 = 1750$ equally-sized grid boxes of $1 \text{ ft} \times 1 \text{ ft}$. For each player, we run an MCMC with $\eta \in \{0, 0.5, \dots, 6.5, 7\}$ for 4000 iterations, where the first 2000 were discarded as burn-in and the remainder was thinned by 10.

Table 4 summarizes the optimal η selected by BIC and the resulting number of clusters. None of the selected $\hat{\eta}$ lies on the boundary, which assures the validity of candidate values of η . For comparison, the number of clusters from the MFM-NHPP model under the same MCMC setting is also included, and we note that MFM-NHPP leads to higher numbers of clusters for most of the players than that of MFM-DPM-NHPP.

Figure 4 and Figure 5 show the estimated shooting intensity surfaces of selected players under MRF-DPM-NHPP and MFM-NHPP, respectively. Compared to the results of MFM-NHPP, it is clear that the MRF-DPM-NHPP model is capable of capturing distant regions that share

Table 4: Basic information (name and the preferred position) of players and the number of clusters given by MRF-DPM-NHPP with the smoothing parameter selected by BIC, and by MFM-NHPP. Player positions: point guard (PG), shooting guard (SG), small forward (SF), power forward (PF), center (C).

Player	Position	MRF-DPM-NHPP		MFM-NHPP
		\widehat{K}_{BIC}	$\widehat{\eta}_{\text{BIC}}$	\widehat{K}
Joel Embiid	C	12	2.5	9
Dwight Howard	C	6	2.5	11
DeAndre Jordan	C	6	4.0	4
Karl-Anthony Towns	C	8	2.5	9
LaMarcus Aldridge	PF	7	2.5	17
Giannis Antetokounmpo	PF	6	3.0	10
Blake Griffin	PF	8	2.5	10
Kristaps Porziņģis	PF	5	2.5	9
Stephen Curry	PG	5	3.0	3
Kyrie Irving	PG	5	3.0	9
Damian Lillard	PG	6	3.0	6
Chris Paul	PG	8	2.5	5
Jimmy Butler	SF	5	3.0	9
Kevin Durant	SF	9	3.0	13
Paul George	SF	6	3.5	8
LeBron James	SF	6	3.0	8
DeMar DeRozan	SG	8	3.0	10
James Harden	SG	8	3.0	11
Klay Thompson	SG	6	5.0	11
Russell Westbrook	SG	5	3.5	10

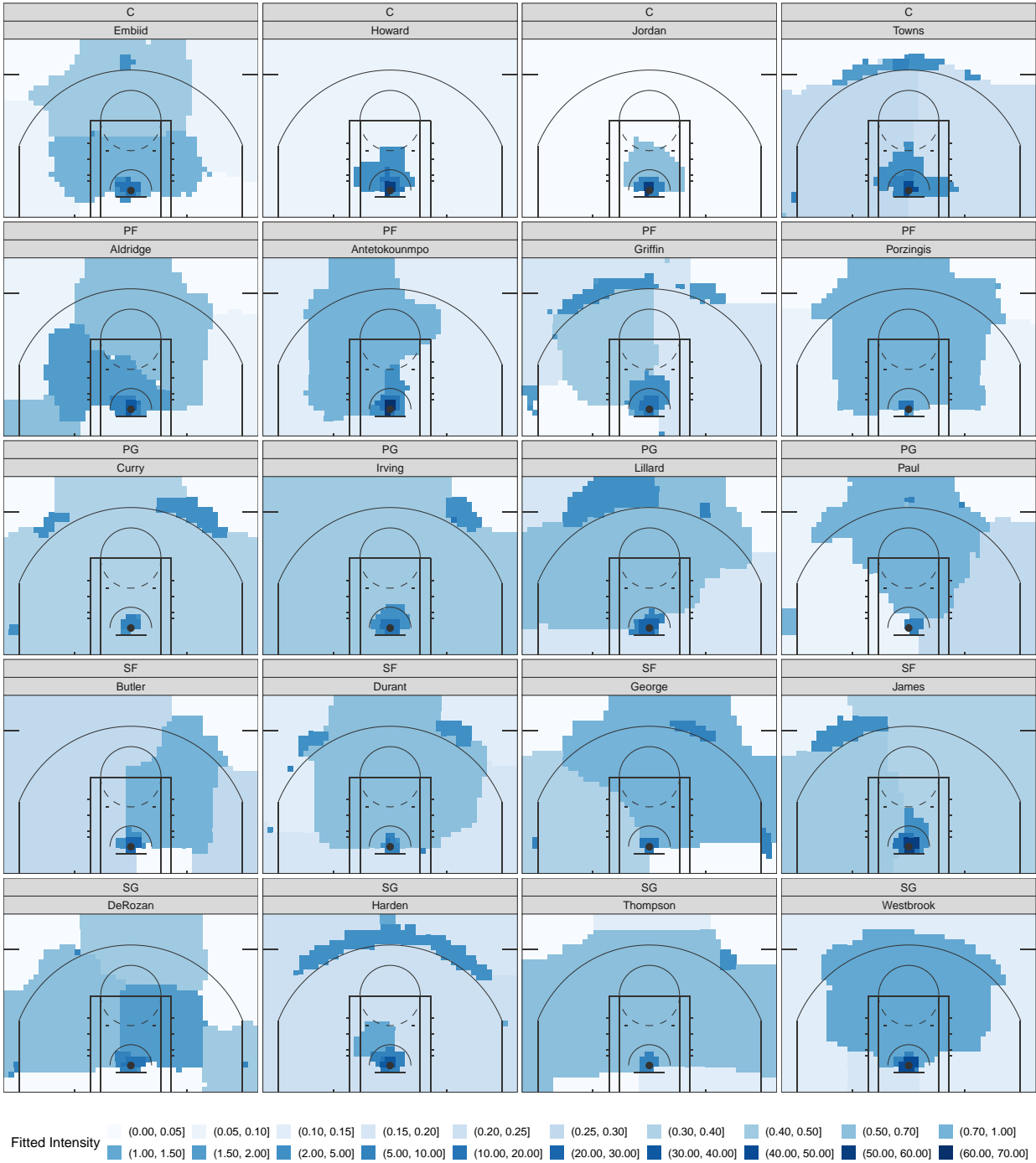


Figure 4: Estimated shooting intensity surfaces of selected players based on MRF-DPM-NHPP.

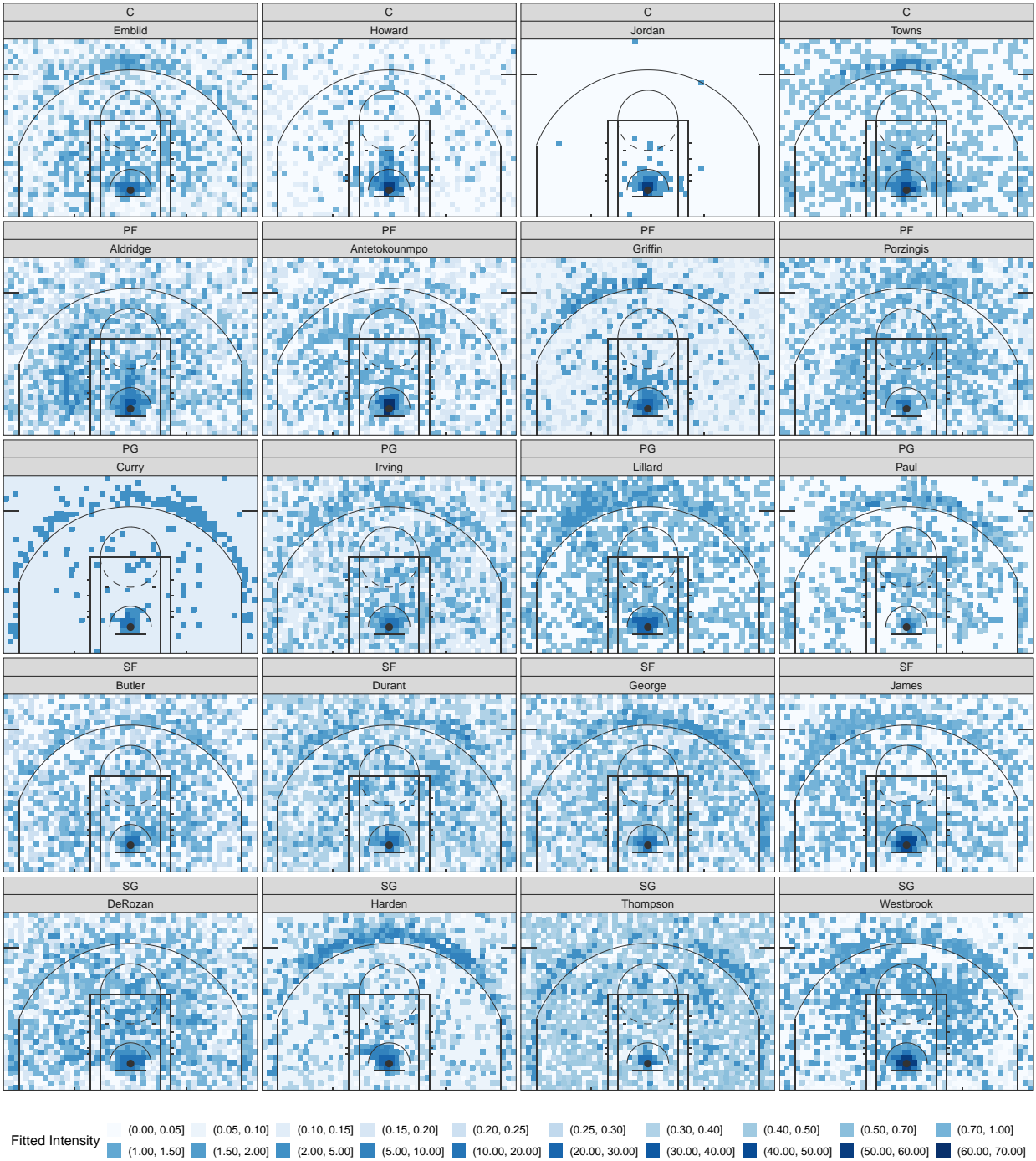


Figure 5: Estimated shooting intensity surfaces of selected players based on MFM-NHPP.

similar shooting intensities while preserving the spatial contiguity, which greatly facilitates the interpretability. Taking Paul George as an example, the estimated shooting intensity surface yielded by MFM-NHPP appears to be too scattered to highlight his preferred shooting regions; the results from the MRF-DPM-NHPP model, however, shows much clearer pattern.

More interesting observations are seen from the estimated shooting intensity surfaces, and we summarize these observations by the preferred positions of selected players. Among those players with preferred position as center, DeAndre Jordan and Dwight Howard rarely make shots outside the low post, while the latter seems to have made more shots from the regions between short corner and the restricted area. On the contrary, Joel Embiid and Karl-Anthony Towns are more versatile as attackers in terms of their shot locations — Joel Embiid can attack from low post, high post, top of the key as well as the *point* (i.e., right outside the middle of the arc); Karl-Anthony Towns' shots are mainly initiated either from the low block or outside the arc (right corner and from point to the wing).

The selected power-forward (PF) players show fairly different shooting styles. The shot locations of Kristaps Porziņģis are very similar to those of Joel Embiid, and Kristaps Porziņģis seems to be less confined to shooting from low post regions compared to Joel Embiid. Both Giannis Antetokounmpo and LaMarcus Aldridge all make substantial amounts of mid-range shots and seldomly make three-point shots, but it is worth highlighting their differences as Giannis Antetokounmpo seems to be more inclined to make shots from the right while LaMarcus Aldridge's mid-range shots are more spread. Interestingly, the former champion of slam dunk contest, Blake Griffin has higher intensity of shooting outside the arc (in particular, from the right corner, and the regions between the wing and the point).

The selected small-forward (SF) players show versatile shot locations but they differ substantially in their three-point shot locations and the intensity of making shots around restricted area. Speaking about the three-point shots, Kevin Durant prefers shooting around left and right wings, both Paul George and Jimmy Butler prefer shooting around the right corner but the former is clearly more comfortable with launching long-range shots, while LeBron James prefers shooting around the left wing. Compared to the other two SF players, LeBron James have higher intensity of making shots around the restricted area.

The difference in the shooting patterns among backcourt (PG and SG) players is substantial.

James Harden, Stephen Curry, Damian Lillard and Kyrie Irving all launch considerable amounts of shots within the restricted area and outside the arc, while James Harden makes shots in almost all regions from right wing to left wing right outside the arc, Stephen Curry and Kyrie Irving make more shots around left wing rather than right wing, Damian Lillard makes more shots around right wing rather than left wing. Compared to the former three players, Chris Paul, Russell Westbrook, DeMar DeRozan and Klay Thompson make more mid-range shots, but from different angles. Specifically, Russell Westbrook makes shots almost everywhere in the middle, Chris Paul’s shots are mainly located in a sector-shaped area in the middle, Demar DeRozan’s shots are more spread to the corners, while Klay Thompson’s shots are almost evenly distributed across the entire study region.

Admittedly, the above analysis is far from being exhaustive. We believe, however, that basketball professionals may leverage the proposed method to better understand the shooting patterns of the players and, therefore, design highly targeted offense and defense tactics.

7 Discussion

The NBA shot location data appear to be modeled by the spatially constrained nonparametric Bayesian model, MRF-DPM-NHPP, reasonably well incorporating local spatial homogeneity. Building upon a combination of Dirichlet process and Markov random field, the proposed method relies on a smoothing parameter η to effectively control the relative contribution of local spatial homogeneity in estimating the globally heterogeneous intensity surface. Statistical inferences are facilitated by a Gibbs sampling algorithm. Selection of the smoothing parameter η is casted as a model selection problem which is handled using standard model selection criteria. Simulation studies show the accuracy of the proposed algorithm and the competitiveness of the model relative to the benchmark MFM-NHPP model (Geng et al., 2019) under several settings in which spatial contiguity is present in the intensity surface. In application to the shot locations of NBA players, the model effectively captures spatial contiguity in shooting intensity surfaces, and provide important insights on their shooting patterns which cannot be obtained from the MFM-NHPP model.

There are several possible directions for further investigation. More sophisticated definition of neighborhood (e.g., higher-order neighborhood, incorporating covariates) than the rook contiguity,

which was used in this study and found to be sufficient here, may be useful for more complex data structure. BIC was found to perform well for the purpose of selecting smoothing parameter η , but it is of substantial interest to develop a fully automated procedure that enables the smoothing parameter to be inferred along with the intensity values and the group membership indicators through a single MCMC run. The NBA players shot pattern modeling admits a natural partition for the region of interest. In general settings, however, it is worth investigating how to effectively partition the space such that the piecewise constant assumption is more plausible. As the number of parameters is proportional to the number of grid boxes, developments of more scalable inference algorithms (e.g., variational inference) are critical for finer grid. Finally, building a group learning model with pooled data from multiple players merits future research from both methodological and applied perspectives.

Acknowledgements

The authors would like to thank Dr. Yishu Xue for sharing the R code of data visualization.

References

- A. Baddeley. Local composite likelihood for spatial point processes. *Spatial Statistics*, 22:261–295, 2017.
- A. Baddeley and R. Turner. spatstat: An r package for analyzing spatial point patterns. *Journal of Statistical Software*, 12(i06), 2005.
- D. Blackwell and J. B. MacQueen. Ferguson distributions via pólya urn schemes. *The Annals of Statistics*, 1(2):353–355, 1973.
- C. Bouveyron, G. Celeux, T. B. Murphy, and A. E. Raftery. *Model-Based Clustering and Classification for Data Science: With Applications in R.*, volume 50. Cambridge University Press, 2019.
- D. B. Dahl. Model-based clustering for expression data via a dirichlet process mixture model. *Bayesian inference for gene expression and proteomics*, 4:201–218, 2006.

- P. J. Diggle. *Statistical analysis of spatial and spatio-temporal point patterns*. CRC press, 2013.
- T. S. Ferguson. A bayesian analysis of some nonparametric problems. *The Annals of Statistics*, pages 209–230, 1973.
- C. Fraley and A. E. Raftery. Model-based clustering, discriminant analysis, and density estimation. *Journal of the American Statistical Association*, 97(458):611–631, 2002.
- W. Fu and P. O. Perry. Estimating the number of clusters using cross-validation. *Journal of Computational and Graphical Statistics*, 29(1):162–173, 2020.
- A. E. Gelfand and D. K. Dey. Bayesian model choice: asymptotics and exact calculations. *Journal of the Royal Statistical Society: Series B (Methodological)*, 56(3):501–514, 1994.
- J. Geng, W. Shi, and G. Hu. Bayesian nonparametric nonhomogeneous poisson process with applications to usgs earthquake data. arXiv e-prints 1907.03186, 2019.
- Y. Guan. A composite likelihood approach in fitting spatial point process models. *Journal of the American Statistical Association*, 101(476):1502–1512, 2006.
- Y. Guan and Y. Shen. A weighted estimating equation approach for inhomogeneous spatial point processes. *Biometrika*, 97(4):867–880, 2010.
- J. M. Hammersley and P. Clifford. Markov fields on finite graphs and lattices. *Unpublished manuscript*, 1971.
- G. Hu, F. Huffer, and M.-H. Chen. New development of Bayesian variable selection criteria for spatial point process with applications. arXiv e-prints 1910.06870, 2019.
- G. Hu, J. Geng, Y. Xue, and H. Sang. Bayesian spatial homogeneity pursuit of functional data: an application to the us income distribution. *arXiv preprint arXiv:2002.06663*, 2020a.
- G. Hu, H.-C. Yang, and Y. Xue. Bayesian group learning for shot selection of professional basketball players. *Stat*, 9(1):e324, 2020b. doi: <https://doi.org/10.1002/sta4.324>. URL <https://onlinelibrary.wiley.com/doi/abs/10.1002/sta4.324>.
- J. Illian, A. Penttinen, H. Stoyan, and D. Stoyan. *Statistical analysis and modelling of spatial point patterns.*, volume 70. John Wiley & Sons, 2008.

- J. Jiao, G. Hu, and J. Yan. A Bayesian joint model for spatial point processes with application to basketball shot chart. *arXiv preprint arXiv:1908.05745*, 2019.
- J. Jiao, G. Hu, and J. Yan. Heterogeneity pursuit for spatial point pattern with application to tree locations: A bayesian semiparametric recourse. *arXiv preprint arXiv:2003.10043*, 2020.
- J. Kubatko, D. Oliver, K. Pelton, and D. T. Rosenbaum. A starting point for analyzing basketball statistics. *Journal of Quantitative Analysis in Sports*, 3(3), 2007.
- F. Li and H. Sang. Spatial homogeneity pursuit of regression coefficients for large datasets. *Journal of the American Statistical Association*, 114(527):1050–1062, 2019.
- G. J. McLachlan and K. E. Basford. *Mixture models: Inference and applications to clustering.*, volume 84. M. Dekker New York, 1988.
- A. Miller, L. Bornn, R. Adams, and K. Goldsberry. Factorized point process intensities: A spatial analysis of professional basketball. In *International conference on machine learning*, pages 235–243, 2014.
- J. W. Miller and M. T. Harrison. Mixture models with a prior on the number of components. *Journal of the American Statistical Association*, 113(521):340–356, 2018.
- J. Møller, A. R. Syversveen, and R. P. Waagepetersen. Log Gaussian Cox processes. *Scandinavian Journal of Statistics*, 25(3):451–482, 1998.
- R. M. Neal. Markov chain sampling methods for dirichlet process mixture models. *Journal of Computational and Graphical Statistics*, 9(2):249–265, 2000.
- P. Orbanz and J. M. Buhmann. Nonparametric bayesian image segmentation. *International Journal of Computer Vision*, 77(1-3):25–45, 2008.
- J. Pitman. Exchangeable and partially exchangeable random partitions. *Probability theory and related fields*, 102(2):145–158, 1995.
- W. M. Rand. Objective criteria for the evaluation of clustering methods. *Journal of the American Statistical Association*, 66(336):846–850, 1971.

- B. J. Reich, J. S. Hodges, B. P. Carlin, and A. M. Reich. A spatial analysis of basketball shot chart data. *The American Statistician*, 60(1):3–12, 2006.
- G. Schwarz. Estimating the dimension of a model. *Annals of Statistics*, 6(2):461–464, 1978.
- D. J. Spiegelhalter, N. G. Best, B. P. Carlin, and A. Van Der Linde. Bayesian measures of model complexity and fit. *Journal of the Royal Statistical Society: Series B (Statistical Methodology)*, 64(4):583–639, 2002.
- M. Teng, F. Nathoo, and T. D. Johnson. Bayesian computation for log-gaussian cox processes: A comparative analysis of methods. *Journal of Statistical Computation and Simulation*, 87(11):2227–2252, 2017.
- W. R. Tobler. A computer movie simulating urban growth in the detroit region. *Economic geography*, 46(sup1):234–240, 1970.
- P. Zhao, H.-C. Yang, D. K. Dey, and G. Hu. Bayesian spatial homogeneity pursuit regression for count value data. *arXiv preprint arXiv:2002.06678*, 2020.